Journal of Solid Mechanics Vol. 8, No. 4 (2016) pp. 895-915

Free and Forced Transverse Vibration Analysis of Moderately Thick Orthotropic Plates Using Spectral Finite Element Method

M.R. Bahrami , S. Hatami *

Civil Engineering Department, Yasouj University, Yasouj, Iran

Received 6 August 2016; accepted 10 October 2016

ABSTRACT

In the present study, a spectral finite element method is developed for free and forced transverse vibration of Levy-type moderately thick rectangular orthotropic plates based on first-order shear deformation theory. Levy solution assumption was used to convert the two-dimensional problem into a one-dimensional problem. In the first step, the governing out-of-plane differential equations are transformed from time domain into frequency domain by discrete Fourier transform theory. Then, the spectral stiffness matrix is formulated, using frequency-dependent dynamic shape functions which are obtained from the exact solution of the governing differential equations. An efficient numerical algorithm, using drawing method is used to extract the natural frequencies. The frequency domain dynamic responses are obtained from solution of the spectral element equation. Also, the time domain dynamic responses are derived by using inverse discrete Fourier transform algorithm. The accuracy and excellent performance of the spectral finite element method is then compared with the results obtained from closed form solution methods in previous studies. Finally, comprehensive results for out-of-plane natural frequencies and transverse displacement of the moderately thick rectangular plates with six different combinations of boundary conditions are presented. These results can serve as a benchmark to compare the accuracy and precision of the numerical methods used.

Keywords : Spectral finite element method; First-order shear deformation theory; Orthotropic plate; Exact solution; Dynamic stiffness matrix; Discrete Fourier transform; Transverse vibration.

1 INTRODUCTION

PLATES are two-dimensional plane structures that are widely used in a variety of engineering fields, such as mechanical, aerospace, shipbuilding, automotive, nuclear, petrochemical, petroleum and civil engineering. Investigating dynamic characteristics of plates and plate structures is necessary to prevent failure and fatigue. Dynamic loads may be created by wave impact, wind gusts, moving vehicles, unbalanced rotating machinery, blast and seismic loads. In general, methods for solving dynamic problems of plates are divided into two categories, namely approximate methods and exact methods.

The exact analytical methods or closed form solutions (CFS) are of considerable importance because of the exact results which they produce. A large number of studies have been carried out using CFS, some of which will be

*Corresponding author. Tel.: +98 917 738 5476; Fax.: +98 74 3322 2917.
E-mail address: hatami@yu.ac.ir (Sh.Hatami).

touched upon here. Reddy and Phan [1] used higher-order shear deformation theory (HSDT) and obtained exact natural frequencies of isotropic, orthotropic and laminated rectangular plates when all edges are simply supported. Xiang and Wei [2] studied free vibration analysis of stepped rectangular Mindlin plates with two opposite edges simply supported and the other two edges having any combination of free, clamped or simply supported boundary conditions. Numerous studies have been carried out by Hosseini Hashemi et al. [3-9] on free vibration of plates including isotropic rectangular plates, functionally graded circular and annular plates, functionally graded rectangular plates based on the first-order shear deformation theory (FSDT) and also, isotropic and functionally graded rectangular plates based on the third-order shear deformation theory (TSDT).

Since the above mentioned CFS do not develop a stiffness matrix, their application is not feasible for the assembly plates and plate structures. To resolve this limitation, the methods based on stiffness matrix analysis can be used in which plates or plate structures are divided into several separate finite strips. The exact finite strip method (EFSM), dynamic stiffness method (DSM) and spectral finite element method (SFEM) are the exact methods that enjoy this capability and thus have been considered by many researchers.

Hatami et al. [10-11] developed an exact finite strip method for laminated composite plates and viscoelastic plates subjected to in-plane forces, using classical plate theory (CPT). By presenting a set of numerical examples, the effect of speed of plate motion and internal supports on the free vibration frequency of the axially moving plates was studied. Using dynamic stiffness method, Boscolo and Banerjee [12-14] presented free vibration analysis of isotropic rectangular plate assemblies and composite plates based on FSDT. As for the capability of the dynamic stiffness method, natural frequencies and mode shapes of L and omega stringer panels and stepped plates are obtained in the works. The HSDT is also used for the development of dynamic stiffness matrix of the composite plates by Leung and Zhou [15] and Fazzolari et al. [16]. Kolarevic et al. [17-18] presented the free vibration analysis of plate assemblies based on FSDT and HSDT. The harmonic responses are obtained for out-of-plane and in-plane vibration of the orthotropic Kirchhoff plate by Ghorbel et al. [19-20].

Spectral finite element method is a combination of dynamic stiffness method and spectral analysis method. The SFEM provides dynamic responses in frequency domain due to the use of dynamic shape functions. In the SFEM, the dynamic responses are being obtained from superposition of a finite number of wave modes corresponding to several discrete frequencies based on the discrete Fourier transform (DFT) theory. In many sciences, including civil engineering, mechanical, soil, hydraulic structures, fluids, etc. the SFEM is used for the analysis of the dynamic behavior of various structures. A set of works carried out by Doyle et al. could be found in Doyle [21]. The SFEM was formulated for the isotropic plates subjected to point and distributed dynamic loads by Lee and Lee [22], axially moving plates with constant speed subjected to uniform in-plane axial tension by Kim et al. [23], composite structures by Chakraborty and Gopalakirshnan [24] and axially moving beam-plates subjected to sudden external thermal loads by Kwon and Lee [25] based on CPT. Wang and Unal [26] developed an efficient and accurate solution to free vibration of stepped thickness rectangular plates with various boundary conditions, which were not limited to Levy-type plates. In their study, the Kantorovich method reduces partial differential equations to a set of linear algebraic equations and provides an analytical approximation solution form for the analysis of structures.

Hajheidari and Mirdamadi [27-28] investigated the free and forced vibration symmetric and non-symmetric cross-ply laminated composite plates based on classical laminated plate theory. The spectral-dynamic stiffness method (S-DSM) was extended to free vibration analysis of the orthotropic composite plates assemblies based on classical lamination plate theory (CLPT) [29-30] and isotropic plates with arbitrary boundary conditions based on CPT [31]. Park and Lee [32] proposed the spectral element model for the symmetric laminated composite plates based on CLPT. Finally, the SFEM was developed for transverse vibration of the moderately thick rectangular plates under impact and moving loads by Shirmohammadi *et al.* [33] and annular Levy-type plates subjected to impact loads by Bahrami et al. [34].

In the present study, an SFEM is developed for free vibration and forced vibration analysis of moderately thick rectangular orthotropic plates having two opposite edges simply supported and remaining edges with any arbitrary boundary conditions (i.e. Levy-type rectangular plates) based on FSDT. The natural frequencies of moderately thick rectangular plates are presented for six combinations of classical boundary conditions, namely CC, CS, FC, FF, FS and SS. The mode shapes for transverse and rotational displacements are plotted. The convergence of the dynamic responses of the plate under dynamic loads for the contribution of the various numbers of half-wavelengths in y-direction and sampling time interval is presented. The dynamic responses to both periodic and impulsive loads in frequency domain and time domain are obtained. The obtained natural frequencies and dynamic responses are compared with available analytical solutions to confirm the validity and exactness of the results.

2 EQUATIONS OF MOTION

Deriving governing differential equations of motion is the first step in the development of spectral finite element matrix for a continuous elastic system. This can be accomplished through various methods such as Newton's second law, the principle of virtual work or Hamilton's principle. Since only transverse (out-of-plane) vibration is of interest, we can just consider inertia forces associated with the transverse translation of the plate without taking into account the inertia forces associated with in-plane translation. Consider a moderately thick rectangular plate of length L_y, width L_x and uniform thickness *h*, as shown in Fig. 1. The displacement fields of plate in *x*-direction, *y*-direction and *z*-direction are represented by $u(x,y,z,t), v(x,y,z,t)$ and $w(x,y,z,t)$, respectively. The displacement fields for moderately thick rectangular plates on the basis of the FSDT, assuming no motion in the membrane $(u_0, v_0 = 0)$ may be expressed as:

$$u(x,y,z,t) = z\phi_x(x,y,t) \quad , \quad v(x,y,z,t) = z\phi_y(x,y,t) \quad , \quad w(x,y,z,t) = w_0(x,y,t) \tag{1}$$

where ϕ_x and ϕ_y are the rotational displacements about the *y* and *x* axes at the middle surface of the plate, respectively, w_0 is the transverse displacement and *t* is the time variable.

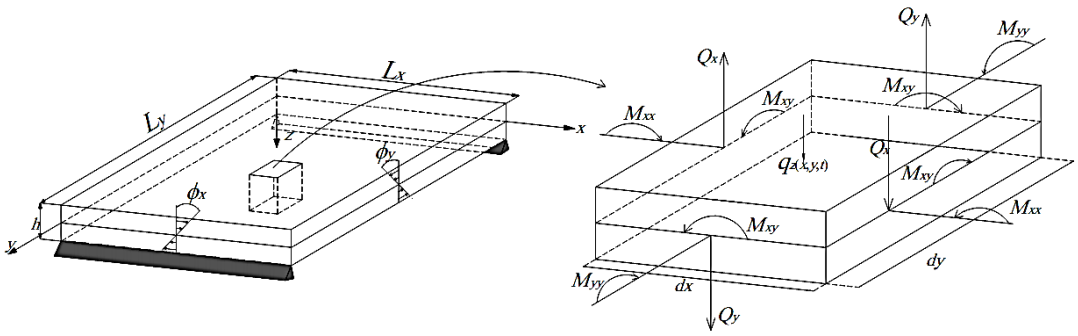

Fig.1
Displacement field, denoted forces and moments and distributed transverse load for a moderately thick rectangular plate.

The governing differential equations of motion are obtained using the Hamilton's principle [35] as follows:

$$\begin{aligned} &Q_{x,x} + Q_{y,y} + q_z - I_0\ddot{w}_0 = 0 \\ &M_{xx,x} + M_{xy,y} - Q_x - I_2\ddot{\phi}_x = 0 \\ &M_{xy,x} + M_{yy,y} - Q_y - I_2\ddot{\phi}_y = 0 \end{aligned} \tag{2}$$

where the comma followed by *x* or *y* parameter denotes differentiation with respect to the *x* or *y*, respectively. Also $I_0 = ph$ and $I_2 = ph^3/12$ are the mass moments of inertia of the plate and ρ is the mass density of plate material. The moments and transverse forces resulting from internal stress according to sign conventions shown in Fig. 1 are defined as follows [35].

$$\begin{Bmatrix} M_{xx} \\ M_{yy} \\ M_{xy} \end{Bmatrix} = \begin{bmatrix} D_{11} & D_{12} & 0 \\ D_{12} & D_{22} & 0 \\ 0 & 0 & D_{66} \end{bmatrix} \begin{Bmatrix} \dfrac{\partial \phi_x}{\partial x} \\ \dfrac{\partial \phi_y}{\partial y} \\ \dfrac{\partial \phi_x}{\partial y} + \dfrac{\partial \phi_y}{\partial x} \end{Bmatrix} \qquad \begin{Bmatrix} Q_y \\ Q_x \end{Bmatrix} = K \begin{bmatrix} A_{44} & 0 \\ 0 & A_{55} \end{bmatrix} \begin{Bmatrix} \dfrac{\partial w_0}{\partial y} + \phi_y \\ \dfrac{\partial w_0}{\partial x} + \phi_x \end{Bmatrix} \tag{3}$$

where K is the shear correction factor, which was obtained by Reissner as 5/6 [36]. Also, the plate stiffnesses A_{ij}, D_{ij} are defined by

$$A_{44} = Q_{44}h \quad , \quad A_{55} = Q_{55}h \quad , \quad D_{11} = \frac{Q_{11}h^3}{12} \quad , \quad D_{12} = \frac{Q_{12}h^3}{12} \quad , \quad D_{22} = \frac{Q_{22}h^3}{12} \quad , \quad D_{66} = \frac{Q_{66}h^3}{12} \tag{4}$$

where

$$Q_{11} = \frac{E_{11}}{1-\nu_{12}\nu_{21}} \quad , \quad Q_{12} = \frac{\nu_{12}E_{22}}{1-\nu_{12}\nu_{21}} \quad , \quad Q_{22} = \frac{E_{22}}{1-\nu_{12}\nu_{21}} \quad , \quad Q_{66} = G_{12} \quad , \quad Q_{44} = G_{23} \quad , \quad Q_{55} = G_{13} \tag{5}$$

where E_{11} is the elastic modulus in the fiber direction, E_{22} the elastic modulus in the direction perpendicular to the fiber, ν_{12} and ν_{21} the Poisson's ratios, G_{12}, G_{13} and G_{23} the shear modulus of each single orthotropic lamina. Substituting Eqs. (3) into Eqs. (2), governing differential equations of motion in terms of displacements w_0, ϕ_x and ϕ_y can be expressed as:

$$\begin{aligned}
&KA_{55}\left(\frac{\partial^2 w_0}{\partial x^2} + \frac{\partial \phi_x}{\partial x}\right) + KA_{44}\left(\frac{\partial^2 w_0}{\partial y^2} + \frac{\partial \phi_y}{\partial y}\right) + q_z = \rho h \ddot{w}_0 \\
&D_{11}\frac{\partial^2 \phi_x}{\partial x^2} + D_{12}\frac{\partial^2 \phi_y}{\partial x \partial y} + D_{66}\left(\frac{\partial^2 \phi_x}{\partial y^2} + \frac{\partial^2 \phi_y}{\partial x \partial y}\right) - KA_{55}\left(\frac{\partial w_0}{\partial x} + \phi_x\right) = \frac{\rho h^3}{12}\ddot{\phi}_x \\
&D_{66}\left(\frac{\partial^2 \phi_x}{\partial x \partial y} + \frac{\partial^2 \phi_y}{\partial x^2}\right) + D_{12}\frac{\partial^2 \phi_x}{\partial x \partial y} + D_{22}\frac{\partial^2 \phi_y}{\partial y^2} - KA_{44}\left(\frac{\partial w_0}{\partial y} + \phi_y\right) = \frac{\rho h^3}{12}\ddot{\phi}_y
\end{aligned} \tag{6}$$

3 SPECTRAL FINITE ELEMENT FORMULATION

The main difficulty using the spectral finite element formulation for the plate is transforming the 2-D problem into a 1-D problem. In this paper, Levy-type solution is used to create a 1-D problem when at least two parallel opposite edges of the plate have simple supports as seen in Fig. 1. The figure shows a Levy-type plate in which two opposite edges ($y = 0$ and L_y) are simply supported and the remaining edges ($x = 0$ and L_x) of the plate can have any arbitrary boundary conditions. The plate behavior in the longitudinal direction (y axis), according to exact analytical solution method, can be represented in the form of a single Fourier series. It should be noted that these functions must satisfy the boundary conditions along two parallel edges at $y = 0$ and L_y . For the Levy-type plates, the simply supported boundary conditions on the two edges $y = 0$ and L_y are defined as follows:

$$w_0(x,0,t) = w_0(x,L_y,t) = 0 \quad , \quad \phi_x(x,0,t) = \phi_x(x,L_y,t) = 0 \quad , \quad M_{yy}(x,0,t) = M_{yy}(x,L_y,t) = 0 \tag{7}$$

From now on, we only need to formulate a 1-D problem (along x axis) in SFEM. Now, displacements of the moderately thick rectangular plate are defined as follows:

$$\phi_x(x,y,t) = \sum_{m=1}^{\infty} \Phi_{xm}(x,t)\sin(k_{ym}y) \quad , \quad \phi_y(x,y,t) = \sum_{m=1}^{\infty} \Phi_{ym}(x,t)\cos(k_{ym}y) \quad , \quad w_0(x,y,t) = \sum_{m=1}^{\infty} W_m(x,t)\sin(k_{ym}y) \tag{8}$$

where $k_{ym} = m\pi / L_y$ and m is the number of half-wavelengths in direction y axis corresponding to terms of Fourier series. Also W_m is modal transverse displacement and Φ_{xm} and Φ_{ym} are modal rotational displacements about the y and x axes, respectively. Similarly, the resultant bending and twisting moments and transverse shear forces are written as:

$$M_{xx}(x,y,t)=\sum_{m=1}^{\infty}M_{xxm}(x,t)\sin(k_{ym}y)\quad,\quad M_{xy}(x,y,t)=\sum_{m=1}^{\infty}M_{xym}(x,t)\cos(k_{ym}y)\quad,\quad Q_{x}(x,y,t)=\sum_{m=1}^{\infty}Q_{xm}(x,t)\sin(k_{ym}y) \tag{9}$$

where M_{xxm} is modal bending moment about the *y* axis, M_{xym} is modal twisting moment and Q_{xm} and Q_{ym}, modal transverse shear forces. On the other hand, based on the Levy-type solution, linear transverse load $q_z(y,t)$ (in direction *y* axis) can be written as a set of half-wavelengths by using single Fourier series, as follows:

$$q_z(y,t)=\sum_{m=1}^{\infty}q_{zm}(t)\sin(k_{ym}y) \tag{10}$$

where q_{zm} is modal linear transverse load and is obtained as follows:

$$q_{zm}(t)=\frac{2}{L_y}\int_0^{L_y}q_z(y,t)\sin(k_{ym}y)\mathrm{d}y \tag{11}$$

3.1 Governing equations in the frequency domain

To obtain frequency-dependent dynamic shape function, it is necessary first to transform governing partial differential equations of motion from the time domain into the frequency domain by DFT. Then the spectral stiffness matrix using dynamic shape function by the force-displacement relation method is achieved. Based on DFT theory, modal displacements W_m,Φ_{xm} and Φ_{ym} expressed in Eqs. (8) are represented in spectral form as follows:

$$\Phi_{xm}(x,t)=\frac{1}{N}\sum_{n=0}^{N-1}\Phi_{xnm}(x,\omega_n)e^{i\omega_n t}\quad,\quad \Phi_{ym}(x,t)=\frac{1}{N}\sum_{n=0}^{N-1}\Phi_{ynm}(x,\omega_n)e^{i\omega_n t}\quad,\quad W_m(x,t)=\frac{1}{N}\sum_{n=0}^{N-1}W_{nm}(x,\omega_n)e^{i\omega_n t} \tag{12}$$

where $i=\sqrt{-1}$ is the imaginary unit, *N* number of samples in the time domain and $\omega_n=2\pi n/T$ is *n*th discrete frequency, where *T* is sampling time window. W_{nm},Φ_{xnm} and Φ_{ynm} are the spectral components (or Fourier coefficients) related to the modal displacements. Similarly all modal force and moments in the spectral forms can be expressed as follows.

$$M_{xxm}(x,t)=\frac{1}{N}\sum_{n=0}^{N-1}M_{xxnm}(x,\omega_n)e^{i\omega_n t}\quad,\quad M_{xym}(x,t)=\frac{1}{N}\sum_{n=0}^{N-1}M_{xynm}(x,\omega_n)e^{i\omega_n t}\quad,\quad Q_{xm}(x,t)=\frac{1}{N}\sum_{n=0}^{N-1}Q_{xnm}(x,\omega_n)e^{i\omega_n t} \tag{13}$$

where Q_{xnm},M_{xxnm} and M_{xynm} are the spectral components (or Fourier coefficients) related to the modal moments and force. Also, based on DFT theory, DFT pair for external applied load $q_{zm}(t)$ is defined by Eqs. (14-15).

$$q_{zm}(t_r)=\frac{1}{N}\sum_{n=0}^{N-1}q_{znm}(\omega_n)e^{i\omega_n t_r}\qquad r=0,1,2,\ldots,N-1 \tag{14}$$

$$q_{znm}(\omega_n)=\sum_{r=0}^{N-1}q_{zm}(t_r)e^{-i\omega_n t_r}\qquad n=0,1,2,\ldots,N-1 \tag{15}$$

where q_{znm} is the DFT coefficients related to the periodic load $q_{zm}(t_r)$ and $t_r=r\Delta t$. In addition, $\Delta t=T/N$ is uniform time interval. Substituting Eqs. (8) and (12) into Eqs. (6) yields a set of coupled ordinary differential equations in the frequency domain as:

$$
\begin{aligned}
&KA_{55}\frac{\mathrm{d}^2W_m}{\mathrm{d}x^2}+(\rho h\omega_n^2-KA_{44}k_{ym}^2)W_m+KA_{55}\frac{\mathrm{d}\Phi_{xm}}{\mathrm{d}x}-KA_{44}k_{ym}\Phi_{ym}=-q_{zm}\\
&D_{11}\frac{\mathrm{d}^2\Phi_{xm}}{\mathrm{d}x^2}+\left(\frac{\rho h^3\omega_n^2}{12}-D_{66}k_{ym}^2-KA_{55}\right)\Phi_{xm}-\left(D_{12}k_{ym}+D_{66}k_{ym}\right)\frac{\mathrm{d}\Phi_{ym}}{\mathrm{d}x}-KA_{55}\frac{\mathrm{d}W_m}{\mathrm{d}x}=0\\
&D_{66}\frac{\mathrm{d}^2\Phi_{ym}}{\mathrm{d}x^2}+\left(\frac{\rho h^3\omega_n^2}{12}-D_{22}k_{ym}^2-KA_{44}\right)\Phi_{ym}+\left(D_{12}k_{ym}+D_{66}k_{ym}\right)\frac{\mathrm{d}\Phi_{xm}}{\mathrm{d}x}-KA_{44}k_{ym}W_m=0
\end{aligned}
\tag{16}
$$

Also by substituting Eqs. (8), (12) and Eqs. (9), (13) into the corresponding relations of the plate (Eqs. 3), the force-displacement relationships in the frequency domain can be expressed as follows.

$$
M_{xxnm}(x,\omega_n)=D_{11}\frac{\mathrm{d}\Phi_{xnm}}{\mathrm{d}x}-D_{12}k_{ym}\Phi_{ynm}\quad,\quad M_{xynm}(x,\omega_n)=D_{66}\left(k_{ym}\Phi_{xnm}+\frac{\mathrm{d}\Phi_{ynm}}{\mathrm{d}x}\right)\quad,\quad Q_{xnm}(x,\omega_n)=A_{55}\left(\frac{\mathrm{d}W_{nm}}{\mathrm{d}x}+\Phi_{xnm}\right)
\tag{17}
$$

3.2 Spectral element equation

3.2.1 General solution of spectral-modal displacements

The dynamic (frequency-dependent) shape functions are obtained from general solution of the governing differential equations. By removing external force ($q_{znm}=0$) from Eqs. (16), the homogeneous equations (in other words, free vibration problem) could be obtained.

$$
\begin{aligned}
&KA_{55}\frac{\mathrm{d}^2W_m}{\mathrm{d}x^2}+(\rho h\omega_n^2-KA_{44}k_{ym}^2)W_m+KA_{55}\frac{\mathrm{d}\Phi_{xm}}{\mathrm{d}x}-KA_{44}k_{ym}\Phi_{ym}=0\\
&D_{11}\frac{\mathrm{d}^2\Phi_{xm}}{\mathrm{d}x^2}+\left(\frac{\rho h^3\omega_n^2}{12}-D_{66}k_{ym}^2-KA_{55}\right)\Phi_{xm}-\left(D_{12}k_{ym}+D_{66}k_{ym}\right)\frac{\mathrm{d}\Phi_{ym}}{\mathrm{d}x}-KA_{55}\frac{\mathrm{d}W_m}{\mathrm{d}x}=0\\
&D_{66}\frac{\mathrm{d}^2\Phi_{ym}}{\mathrm{d}x^2}+\left(\frac{\rho h^3\omega_n^2}{12}-D_{22}k_{ym}^2-KA_{44}\right)\Phi_{ym}+\left(D_{12}k_{ym}+D_{66}k_{ym}\right)\frac{\mathrm{d}\Phi_{xm}}{\mathrm{d}x}-KA_{44}k_{ym}W_m=0
\end{aligned}
\tag{18}
$$

Assume the general solutions of Eqs. (18) is as follows.

$$
W_{nm}=\alpha b_{nm}e^{k_{xnm}x}\quad,\quad \Phi_{xnm}=b_{nm}e^{k_{xnm}x}\quad,\quad \Phi_{ynm}=\beta b_{nm}e^{k_{xnm}x}
\tag{19}
$$

where k_{xnm} are wavenumbers in direction x axis and b_{nm} the constant coefficient. Substituting Eqs. (19) into Eqs. (18) an eigenvalue problem is obtained.

$$
\begin{bmatrix}T_{11}&T_{12}&T_{13}\\T_{21}&T_{22}&T_{23}\\T_{31}&T_{32}&T_{33}\end{bmatrix}\begin{Bmatrix}\alpha\\1\\\beta\end{Bmatrix}b_{nm}=\begin{Bmatrix}0\\0\\0\end{Bmatrix}
\tag{20}
$$

where

$$
\begin{aligned}
&T_{11}=KA_{55}k_{xnm}^2+\rho h\omega_n^2-KA_{44}k_{ym}^2\quad,\quad T_{12}=KA_{55}k_{xnm}\quad,\quad T_{13}=-KA_{44}k_{ym}\\
&T_{21}=-KA_{55}k_{xnm}\quad,\quad T_{22}=D_{11}k_{xnm}^2+\frac{\rho h^3\omega_n^2}{12}-D_{66}k_{ym}^2-KA_{55}\quad,\quad T_{23}=-\left(D_{12}+D_{66}\right)k_{ym}k_{xnm}\\
&T_{31}=-KA_{44}k_{ym}\quad,\quad T_{32}=\left(D_{12}+D_{66}\right)k_{ym}k_{xnm}\quad,\quad T_{33}=D_{66}k_{xnm}^2+\frac{\rho h^3\omega_n^2}{12}-D_{22}k_{ym}^2-KA_{44}
\end{aligned}
\tag{21}
$$

The algebraic Eq. (20) has a nontrivial solution, which is obtained by setting determinant of the coefficients matrix as zero. Hence, after simplification, it yields a six order polynomial in terms of wavenumbers.

$$m_1 k_{xnm}^6 + m_2 k_{xnm}^4 + m_3 k_{xnm}^2 + m_4 = 0 \tag{22}$$

where

$$\begin{aligned}
m_1 &= KA_{55}D_{11}D_{66} \\
m_2 &= -KA_{44}D_{11}\left(KA_{55} + D_{66}k_{ym}^2\right) + D_{11}D_{66}\rho h\omega_n^2 + \frac{1}{12}KA_{55}\begin{pmatrix} 12D_{12}^2k_{ym}^2 - 12D_{11}D_{22}k_{ym}^2 + 24D_{12}D_{66}k_{ym}^2 + \\ D_{11}\rho h^3\omega_n^2 + D_{66}\rho h^3\omega_n^2 \end{pmatrix} \\
m_3 &= \frac{1}{144}\begin{bmatrix} 12\rho h\omega_n^2\left(12D_{12}^2k_{ym}^2 - 12D_{11}D_{22}k_{ym}^2 + 24D_{12}D_{66}k_{ym}^2 + D_{11}\rho h^3\omega_n^2 + D_{66}\rho h^3\omega_n^2\right) + \\ 12A_{44}K\begin{pmatrix} 24KA_{55}D_{12}k_{ym}^2 + 48KA_{55}D_{66}k_{ym}^2 - 12D_{12}^2k_{ym}^4 + 12D_{11}D_{22}k_{ym}^4 - 24D_{12}D_{66}k_{ym}^4 - \\ 12D_{11}\rho h\omega_n^2 - KA_{55}\rho h^3\omega_n^2 - D_{11}k_{ym}^2\rho h^3\omega_n^2 - D_{66}k_{ym}^2\rho h^3\omega_n^2 \end{pmatrix} + \\ KA_{55}\left(\rho h\omega_n^2\left\langle\rho h^5\omega_n^2 - 12D_{66}(12 + h^2k_{ym}^2)\right\rangle + 12D_{22}\left\langle 12D_{66}k_{ym}^4 - \rho h^3\omega_n^2k_{ym}^2\right\rangle\right) \end{bmatrix} \\
m_4 &= -\frac{1}{144}\left(12KA_{55} + 12D_{66}k_{ym}^2 - \rho h^3\omega_n^2\right)\left\{\rho h\omega_n^2\left(\rho h^3\omega_n^2 - 12D_{22}k_{ym}^2\right) + KA_{44}\left[12D_{22}k_{ym}^4 - \left(12 + h^2k_{ym}^2\right)\rho h\omega_n^2\right]\right\}
\end{aligned} \tag{23}$$

Eq. (22) is known as the dispersion relation or spectrum relation. The roots (i.e. wavenumbers) of this equation are obtained as follows.

$$k_{xnm1,2} = \pm\sqrt{-\frac{1}{3}b_1 + I + J}, \quad k_{xnm3,4} = \pm\sqrt{-\frac{1}{3}b_1 - \frac{1+i\sqrt{3}}{2}I - \frac{1-i\sqrt{3}}{2}J}, \quad k_{xnm5,6} = \pm\sqrt{-\frac{1}{3}b_1 - \frac{1-i\sqrt{3}}{2}I - \frac{1+i\sqrt{3}}{2}J} \tag{24}$$

where

$$\begin{aligned}
&b_1 = \frac{m_2}{m_1} \quad , \quad b_2 = \frac{m_3}{m_1} \quad , \quad b_3 = \frac{m_4}{m_1} \quad , \quad p = \frac{3b_2 - b_1^2}{9} \quad , \quad q = \frac{2b_1^3 - 9b_1b_2 + 27b_3}{27} \\
&I = \sqrt[3]{\frac{1}{2}\left(-q - \sqrt{4p^3 + q^2}\right)} \quad , \quad J = \sqrt[3]{\frac{1}{2}\left(-q + \sqrt{4p^3 + q^2}\right)}
\end{aligned} \tag{25}$$

The coefficients α and β corresponding to each wavenumber obtained from Eqs. (20) are as follows.

$$\begin{aligned}
\alpha_i &= -\frac{K\left[12KA_{44}A_{55} - 12A_{44}D_{11}k_{xnmi}^2 + 12A_{44}D_{66}k_{ym}^2 - A_{44}\rho h^3\omega_n^2 + 12A_{55}k_{xnmi}^2\left(D_{12} + D_{66}\right)\right]}{12k_{xnmi}\left[K^2A_{44}A_{55} + \left(D_{12} + D_{66}\right)\left(KA_{55}k_{xnmi}^2 + \rho h\omega_n^2 - KA_{44}k_{ym}^2\right)\right]} \\
\beta_i &= -\frac{\left[-K^2A_{55}^2k_{xnmi}^2 - \left(KA_{55}k_{xnmi}^2 - KA_{44}k_{ym}^2 + \rho h\omega_n^2\right)\left(D_{11}k_{xnmi}^2 - KA_{55} - D_{66}k_{ym}^2 + \frac{1}{12}\rho h^3\omega_n^2\right)\right]}{\left[K^2A_{44}A_{55}k_{ym}k_{xnmi} + k_{ym}k_{xnmi}\left(D_{12} + D_{66}\right)\left(KA_{55}k_{xnmi}^2 - KA_{44}k_{ym}^2 + \rho h\omega_n^2\right)\right]}
\end{aligned} \tag{26}$$

Finally, the general solutions of Eqs. (18) is presented as follows.

$$\Phi_{xnm}=\sum_{i=1}^{6}b_{nmi}\,e^{k_{xnmi}\,x}=E_{nm}^{\mathrm{T}}(x,\omega_n)b_{nm}\quad,\quad \Phi_{ynm}=\sum_{i=1}^{6}\beta_i b_{nmi}\,e^{k_{xnmi}\,x}=E_{nm}^{\mathrm{T}}(x,\omega_n)\beta_p b_{nm}$$
$$W_{nm}=\sum_{i=1}^{6}\alpha_i b_{nmi}\,e^{k_{xnmi}\,x}=E_{nm}^{\mathrm{T}}(x,\omega_n)a_p b_{nm} \tag{27}$$

where

$$E_{nm}^{\mathrm{T}}(x,\omega_n)=\begin{bmatrix}e^{k_{xnm1}\,x} & e^{k_{xnm2}\,x} & e^{k_{xnm3}\,x} & e^{k_{xnm4}\,x} & e^{k_{xnm5}\,x} & e^{k_{xnm6}\,x}\end{bmatrix}$$
$$b_{nm}=\begin{bmatrix}b_{nm1} & b_{nm2} & b_{nm3} & b_{nm4} & b_{nm5} & b_{nm6}\end{bmatrix}^{\mathrm{T}} \tag{28}$$

and

$$\alpha_p=\mathrm{diag}[\alpha_i]=\mathrm{diag}\begin{bmatrix}\alpha_1 & \alpha_2 & \alpha_3 & \dots & \alpha_6\end{bmatrix}_{6\times 6}\quad,\quad \beta_p=\mathrm{diag}[\beta_i]=\mathrm{diag}\begin{bmatrix}\beta_1 & \beta_2 & \beta_3 & \dots & \beta_6\end{bmatrix}_{6\times 6} \tag{29}$$

3.2.2 Spectral-modal nodal DOFs vector

For a spectral finite element shown in Fig. 2(b), the geometric boundary conditions must be satisfied at the element nodes ($x=x_1$ and $x=x_2$). The geometric boundary conditions include the transverse displacement and rotational displacements about the *y* and *x* axes. The spectral-modal nodal degrees of freedom (DOFs) for the moderately thick rectangular plate element are specified in Fig. 2(b).

The spectral-modal nodal DOFs vector d_{nm} can be defined by applying the geometric boundary conditions, as follows.

$$d_{nm}=\left\{W_{nm1}\quad \Phi_{xnm1}\quad \Phi_{ynm1}\quad W_{nm2}\quad \Phi_{xnm2}\quad \Phi_{ynm2}\right\}^{\mathrm{T}}=\left\{W_{nm}(x_1)\quad \Phi_{xnm}(x_1)\quad \Phi_{ynm}(x_1)\quad W_{nm}(x_2)\quad \Phi_{xnm}(x_2)\quad \Phi_{ynm}(x_2)\right\}^{\mathrm{T}} \tag{30}$$

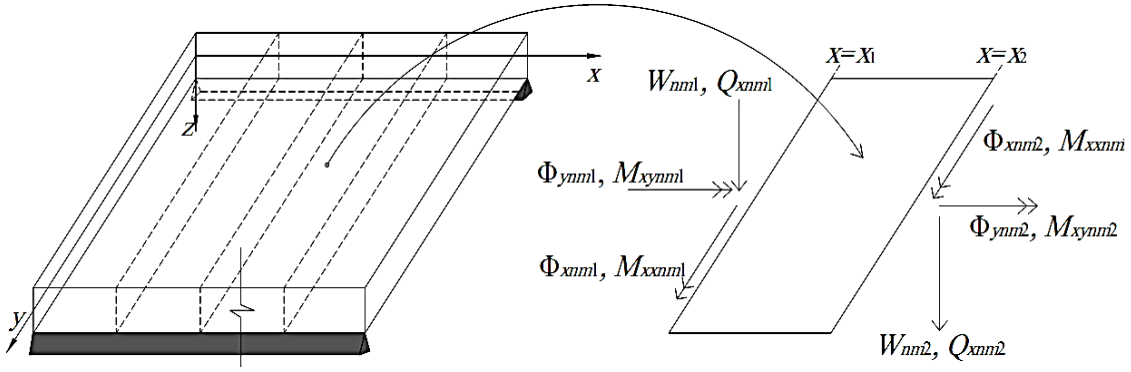

(a) dividing the plate to some elements (b) spectral finite element

Fig.2
Sign conventions spectral-modal nodal DOFs and forces.

Substituting Eqs. (27) into Eq. (30) yields the relationship as:

$$d_{nm}=G_{nm}(\omega_n)\,b_{nm} \tag{31}$$

where

$$G_{nm}(\omega_n)=\begin{bmatrix} \alpha_1 e^{k_{xnm1}x_1} & \alpha_2 e^{k_{xnm2}x_1} & \dots & \alpha_6 e^{k_{xnm6}x_1} \\ e^{k_{xnm1}x_1} & e^{k_{xnm2}x_1} & \dots & e^{k_{xnm6}x_1} \\ \beta_1 e^{k_{xnm1}x_1} & \beta_2 e^{k_{xnm2}x_1} & \dots & \beta_6 e^{k_{xnm6}x_1} \\ \alpha_1 e^{k_{xnm1}x_2} & \alpha_2 e^{k_{xnm2}x_2} & \dots & \alpha_6 e^{k_{xnm6}x_2} \\ e^{k_{xnm1}x_2} & e^{k_{xnm2}x_2} & \dots & e^{k_{xnm6}x_2} \\ \beta_1 e^{k_{xnm1}x_2} & \beta_2 e^{k_{xnm2}x_2} & \dots & \beta_6 e^{k_{xnm6}x_2} \end{bmatrix}_{6\times 6} \tag{32}$$

3.2.3 Dynamic shape functions

By eliminating the constant vector b_{nm} from Eqs. (27) by using Eq. (31), the general solutions of the governing ordinary differential equations of motion in the frequency domain (relations Eqs.(18)) in terms of the spectral-modal nodal DOFs vector d_{nm} are expressed as follows:

$$W_{nm}=N_{Wnm}^{\mathrm{T}}d_{nm} \quad , \quad \Phi_{xnm}=N_{\Phi xnm}^{\mathrm{T}}d_{nm} \quad , \quad \Phi_{ynm}=N_{\Phi ynm}^{\mathrm{T}}d_{nm} \tag{33}$$

where $N_{Wnm}^{\mathrm{T}}, N_{\Phi xnm}^{\mathrm{T}}$ and $N_{\Phi ynm}^{\mathrm{T}}$ are the dynamic (frequency-dependent) shape functions related to spectral-modal displacements w_{nm}, Φ_{xnm} and Φ_{ynm}, respectively. They are obtained from the exact solution of the governing differential equations and are defined as follows. The dynamic shape functions are 1-by-6 matrices.

$$N_{Wnm}^{\mathrm{T}}(x,\omega_n)=E_{nm}^{\mathrm{T}}\alpha_p G_{nm}^{-1} \, , \quad N_{\Phi xnm}^{\mathrm{T}}(x,\omega_n)=E_{nm}^{\mathrm{T}}G_{nm}^{-1} \, , \quad N_{\Phi ynm}^{\mathrm{T}}(x,\omega_n)=E_{nm}^{\mathrm{T}}\beta_p G_{nm}^{-1} \tag{34}$$

3.2.4 Spectral-modal nodal forces vector

Substituting Eqs. (27) into Eq. (17), the force-displacement relationships in the frequency domain can be rewritten as follows:

$$\begin{aligned} &\hat{M}_{xxnm}=\sum_{i=1}^{6} b_{nmi}\left[D_{11}k_{xnmi}-D_{12}k_{ym}\beta_i\right]e^{k_{xnmi}x} \quad , \quad \hat{M}_{xynm}=\sum_{i=1}^{6} b_{nmi}\left[D_{66}\left(k_{ym}+\beta_i k_{xnmi}\right)\right]e^{k_{xnmi}x} \\ &\hat{Q}_{xnm}=\sum_{i=1}^{6} b_{nmi}\left[A_{55}\left(\alpha_i k_{xnmi}+1\right)\right]e^{k_{xnmi}x} \end{aligned} \tag{35}$$

For a spectral finite element shown in Fig. 2(b), the natural boundary conditions at the element nodes ($x=x_1$ and $x=x_2$) must be satisfied. The natural boundary conditions in the frequency domain include the spectral-modal transverse shear force Q_{xnm}, spectral-modal bending moment M_{xxnm} and spectral-modal twisting moment M_{xynm}. The spectral-modal nodal force and moments for the moderately thick rectangular plate element are shown in Fig. 2(b). The spectral-modal nodal forces vector f_{nm} can be obtained by applying the natural boundary conditions, and given the sign conventions used in the theory of the plate (shown in Fig. 1), they are written as follows:

$$\begin{aligned} f_{nm}&=\left\{Q_{xnm1} \quad M_{xxnm1} \quad M_{xynm1} \quad Q_{xnm2} \quad M_{xxnm2} \quad M_{xynm2}\right\}^{\mathrm{T}} \\ &=\left\{-Q_{xnm}(x_1) \quad -M_{xxnm}(x_1) \quad M_{xynm}(x_1) \quad Q_{xnm}(x_2) \quad M_{xxnm}(x_2) \quad -M_{xynm}(x_2)\right\}^{\mathrm{T}} \end{aligned} \tag{36}$$

Substituting Eqs. (35) into Eq. (36) yields the relationship as:

$$f_{nm}=R_{nm}(\omega_n)b_{nm} \tag{37}$$

where

$$R_{nm}(\omega_n)=\begin{bmatrix} -A_1 e^{k_{xnm1}x_1} & -A_2 e^{k_{xnm2}x_1} & \dots & -A_6 e^{k_{xnm6}x_1} \\ -B_1 e^{k_{xnm1}x_1} & -B_2 e^{k_{xnm2}x_1} & \dots & -B_6 e^{k_{xnm6}x_1} \\ -C_1 e^{k_{xnm1}x_1} & -C_2 e^{k_{xnm2}x_1} & \dots & -C_6 e^{k_{xnm6}x_1} \\ A_1 e^{k_{xnm1}x_2} & A_2 e^{k_{xnm2}x_2} & \dots & A_6 e^{k_{xnm6}x_2} \\ B_1 e^{k_{xnm1}x_2} & B_2 e^{k_{xnm2}x_2} & \dots & B_6 e^{k_{xnm6}x_2} \\ C_1 e^{k_{xnm1}x_2} & C_2 e^{k_{xnm2}x_2} & \dots & C_6 e^{k_{xnm6}x_2} \end{bmatrix}_{6\times 6} \tag{38}$$

and

$$A_i = A_{55}\,(\alpha_i k_{xnmi}+1) \quad , \quad B_i = D_{11}k_{xnmi} - D_{12}k_{ym}\beta_i \quad , \quad C_i = -D_{66}\left(k_{ym}+\beta_i k_{xnmi}\right) \quad , \quad \left(i=1,2,\dots,6\right) \tag{39}$$

3.2.5 Spectral stiffness matrix

Eliminating the constant coefficients vector b_{nm} from Eq. (37) using Eq. (31) gives the relationship between the spectral-modal nodal forces vector f_{nm} and the spectral-modal nodal DOFs vector d_{nm} as follows. This relationship is known in the literature as spectral element equation.

$$f_{nm} = S_{nm} d_{nm} \tag{40}$$

where

$$S_{nm}(\omega_n) = R_{nm} G_{nm}^{-1} \tag{41}$$

The matrix S_{nm} is known as exact dynamic (frequency-dependent) stiffness matrix. In the literature it is often called spectral element matrix or spectral stiffness matrix. Also the matrix S_{nm} is a six-by-six and symmetric matrix. The present spectral stiffness matrix is formulated for the moderately thick rectangular plate element based on FSDT.

4 SPECTRAL ELEMENT ANALYSIS

4.1 Global spectral stiffness matrix

The first step in spectral element analysis is dividing the plate into several individual spectral finite elements due to boundary conditions, and geometric and mechanical properties of plate material. Also, if any discontinuities exist in the external loads applied to the plate, due to loading conditions, a greater number of spectral finite elements may be needed. Following that, the spectral-modal nodal DOFs and forces at each node of the spectral finite elements could be defined. The spectral element equation explained in Eq. (40) can be assembled by using a method similar to that used in the conventional finite element method. Finally, global system equation is given as follows:

$$f_{gnm} = S_{gnm}(\omega_n)\, d_{gnm} \tag{42}$$

where S_{gnm} is the global spectral stiffness matrix, d_{gnm} is the global spectral-modal nodal DOFs vector and f_{gnm} is the global spectral-modal nodal forces vector. Fig. 3 shows six different combinations of boundary conditions, namely CC, CS, FC, FF, FS, SS. The boundary conditions of two parallel edges at $y=0$ and L_y that are simply supported are not written for brevity. As a sample, for CC boundary condition, W_{nm}, Φ_{xnm} and Φ_{ynm} according to the first and end node lines are zero, thus the relevant members are eliminated from S_{gnm} matrix and from d_{gnm} and

f_{gnm} vectors. After applying the associated boundary conditions on the assembled set of equations, the final form of the global system equation is obtained.

$$\bar{f}_{gnm} = \bar{S}_{gnm}(\omega_n)\bar{d}_{gnm} \tag{43}$$

4.2 Natural frequency and mode shapes

By setting $\bar{f}_{gnm}$ to zero, the eigenvalue problem for free vibration of the intended plate can be obtained.

$$\bar{S}_{gnm}(\omega_n)\bar{d}_{gnm} = 0 \tag{44}$$

By setting the determinant of $\bar{S}_{gnm}$ to zero, the natural frequencies, ω_{NAT}, are determined.

$$\det\left(\bar{S}_{gnm}(\omega_n)\right) = 0 \tag{45}$$

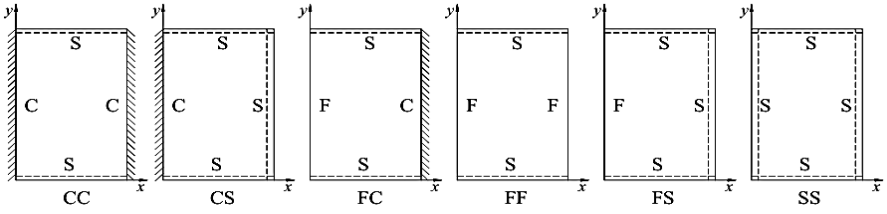

Fig.3
Six combinations of boundary conditions for moderately thick rectangular plate.

Eq. (44) is a transcendental eigenvalue problem. Therefore, the traditional procedures for solving the linear eigenvalue problem are not applicable. In earlier publications, various methods including Wittrick-Williams algorithm and method of trial and error to obtain the natural frequencies of Eq. (45) were suggested. In the present paper an efficient numerical algorithm using drawing method described by Hatami et al. [10] is used. In this procedure, the variation of stiffness matrix determinant $\det\left(\bar{S}_{gnm}\right)$ in logarithmic scale versus discrete frequencies ω_n is plotted for different values of half-wavelengths, *m*. The points on the horizontal axis in which the logarithmic function tends to negative infinity are natural frequencies. Substituting these natural frequencies into Eq. (44), corresponding mode shapes can be computed.

4.3 Frequency Response Functions (FRF)

To continue the previous formulation, the global spectral-modal nodal DOFs vector $\bar{d}_{gnm}$ can be computed form Eq. (43) and then the spectral-modal nodal DOFs vector d_{nm} associated with the spectral finite element with respect to $\bar{d}_{gnm}$ can be written as follows:

$$d_{nm} = L\bar{d}_{gnm} = L\,\bar{S}_{gnm}^{-1}\,\bar{f}_{gnm} \tag{46}$$

where *L* is the locator matrix. Substituting Eq. (46) into Eqs. (33), frequency domain dynamic responses are obtained as follows:

$$W_{nm} = H_{Wnm}^{\mathrm{T}}\bar{f}_{gnm} \quad , \quad \Phi_{xnm} = H_{\Phi xnm}^{\mathrm{T}}\bar{f}_{gnm} \quad , \quad \Phi_{ynm} = H_{\Phi ynm}^{\mathrm{T}}\bar{f}_{gnm} \tag{47}$$

with

$$H^{\mathrm{T}}_{Wnm}(x,\omega_n)=N^{\mathrm{T}}_{Wnm}\,L\bar{S}^{-1}_{gnm}\ ,\quad H^{\mathrm{T}}_{\Phi xnm}(x,\omega_n)=N^{\mathrm{T}}_{\Phi xnm}\,L\bar{S}^{-1}_{gnm}\ ,\quad H^{\mathrm{T}}_{\Phi ynm}(x,\omega_n)=N^{\mathrm{T}}_{\Phi ynm}\,L\bar{S}^{-1}_{gnm} \tag{48}$$

where $H^{\mathrm{T}}_{Wnm}, H^{\mathrm{T}}_{\Phi xnm}$ and $H^{\mathrm{T}}_{\Phi ynm}$ are the frequency response functions for the spectral-modal displacements W_{nm}, Φ_{xnm} and Φ_{ynm}, respectively.

4.4 Frequency domain dynamic responses

The spectral components related to the time domain displacements W_n, Φ_{yn} and Φ_{xn} can be calculated for each specific coordinate (x,y) of the plate as a set of half-wavelengths in direction y axis (single Fourier series). If these functions are calculated for the discrete frequencies, they are known as frequency domain dynamic responses, which, using Eqs. (47) can be obtained as follows:

$$\begin{aligned}&\Phi_{xn}(x,y,\omega_n)=\sum_{m=1}^{\infty}\Phi_{xnm}(x,\omega_n)\sin(k_{ym}y)\quad ,\quad \Phi_{yn}(x,y,\omega_n)=\sum_{m=1}^{\infty}\Phi_{ynm}(x,\omega_n)\cos(k_{ym}y)\\&W_n(x,y,\omega_n)=\sum_{m=1}^{\infty}W_{nm}(x,\omega_n)\sin(k_{ym}y)\end{aligned} \tag{49}$$

4.5 Time domain dynamic responses

Lastly, using Eqs. (12) (in other words, inverse DFT algorithm) modal displacements and then using Eqs. (8) (in other words, single Fourier series expansion) time domain displacements responses can be obtained. Also, combining Eqs. (8) and (12) can be directly used as follows:

$$\begin{aligned}&\phi_x=\frac{1}{N}\sum_{n=0}^{N-1}\sum_{m=1}^{\infty}\Phi_{xnm}(x,\omega_n)\sin(k_{ym}y)e^{i\omega_n t}\quad ,\quad \phi_y=\frac{1}{N}\sum_{n=0}^{N-1}\sum_{m=1}^{\infty}\Phi_{ynm}(x,\omega_n)\cos(k_{ym}y)e^{i\omega_n t}\\&w_0=\frac{1}{N}\sum_{n=0}^{N-1}\sum_{m=1}^{\infty}W_{nm}(x,\omega_n)\sin(k_{ym}y)e^{i\omega_n t}\end{aligned} \tag{50}$$

5 NUMERICAL RESULTS AND DISCUSSION

The proposed SFEM is programmed in the environment of Mathematica to obtain the natural frequencies, mode shapes and dynamic responses in the frequency and time domain. The accuracy and excellent performance of the SFEM against the results available in the literature are investigated.

5.1 Free vibration

At first, exact frequencies of free transverse vibration of Levy-type rectangular plates are calculated based on FSDT with various boundary conditions. For this purpose, an isotropic rectangular plate ($L_x=2L_y$) with width to thickness ratio of 10 ($L_x/h=10$) is considered and the shear correction factor and Poisson's ratio are assumed as13/15 and 0.3, respectively. Fig. 4 shows the variation of Log(Abs(Det[$\bar{S}_{gnm}(k_{ym},\omega_n)$])) with respect to frequency parameter $\bar{\omega}$ for different values of half-wavelengths along y-direction, m. As mentioned in Section 4.2, the points on the horizontal axis in which the logarithmic function tends to negative infinity are natural frequencies.

The subscript m in $\bar{\omega}_{mn}$ is the number of half-wavelengths in the y-direction and the subscript n is the root number in the characteristic function of Eq. (45). It should be mentioned that there is an infinite number of roots for this function. As shown in Fig. 4(a), for CC boundary condition, the first, the second and the third frequency

parameters correspond to a single sinusoidal wave in direction of y axis ($m=1$); and the fourth and the fifth frequency parameters are associated with double wave ($m=2$).

In Table 1., the first nine frequency parameters are compared with the results of exact closed form solution offered by Hosseini Hashemi and Arsanjani [3] based on FSDT for different boundary conditions (CC, CS, FC, FF, FS, SS). Maximum of two finite elements in x-direction are used to obtain the results of spectral finite element formulation. As it could be observed, proposed SFEM with a minimum number of finite elements produces exact results, compared with other exact analytical methods available. Therefore, this procedure could effectively be used for the purpose of modeling plate structures with more than one finite element (for example, multi-span plates, stepped thickness plates and plates with internal support).

Table 2. shows the dimensionless natural frequencies of the Levy-type square orthotropic plate obtained by the spectral finite element method based on FSDT. These plate having the mechanical properties $E_{11}=20.83\times10^6$, $E_{22}=10.94\times10^6, G_{12}=6.10\times10^6, G_{13}=3.71\times10^6, G_{23}=6.19\times10^6, v_{12}=0.23$. For confidence, these results are compared with the results reported in Ref. [1] according to FSDT, HSDT and 3D elasticity theory.

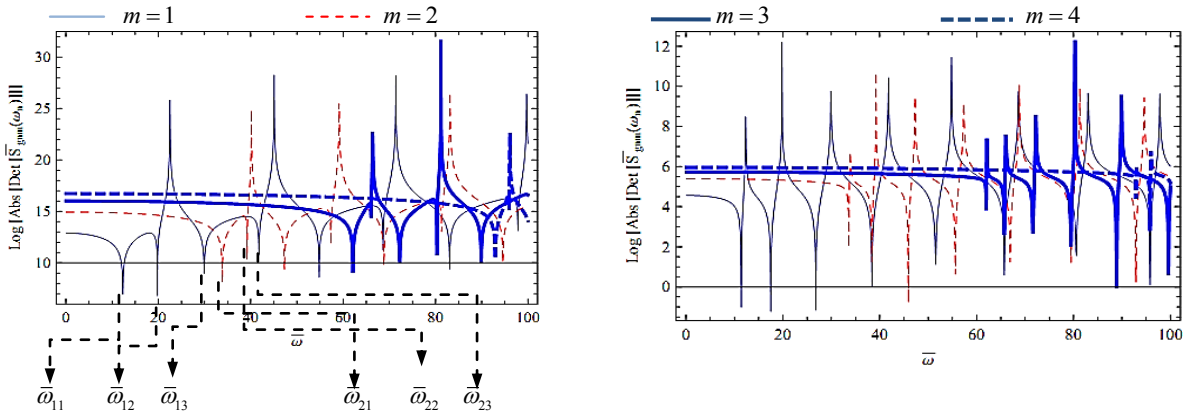

(a) CC (b) SS

Fig.4
Natural frequencies extraction of moderately thick square isotropic plate for boundary conditions CC and SS.

Table 1
Comparison of the dimensionless natural frequencies $\bar{\omega}=\omega_n L_y^2\sqrt{\rho h/D}$ a Levy-type isotropic plate when $L_x/h=10$, $L_x/L_y=2$, $v=0.3, K=13/15$.

B.C.	Method	Mode sequences								
		1	2	3	4	5	6	7	8	9
CC	EFSM	12.3152	19.7988	29.9258	33.8397	39.2032	41.7813	47.2796	54.8076	57.3380
	(m,n)	(1,1)	(1,2)	(1,3)	(2,1)	(2,2)	(1,4)	(2,3)	(1,5)	(2,4)
	CFS [3]	12.3152	19.7988	29.9258	33.8397	39.2032	41.7813	47.2796	54.8076	57.3380
CS	EFSM	11.8061	18.6005	28.3427	33.7085	38.7801	40.0930	46.5758	53.1956	56.4568
	(m,n)	(1,1)	(1,2)	(1,3)	(2,1)	(2,2)	(1,4)	(2,3)	(1,5)	(2,4)
	CFS [3]	11.8061	18.6005	28.3427	33.7085	38.7801	40.0930	46.5758	53.1956	56.4568
FC	EFSM	9.6782	13.9934	21.5678	31.6896	32.0545	35.3839	41.5112	43.6674	49.9152
	(m,n)	(1,1)	(1,2)	(1,3)	(1,4)	(2,1)	(2,2)	(2,3)	(1,5)	(2,4)
	CFS [3]	9.6782	13.9934	21.5678	31.6896	32.0545	35.3839	41.5112	43.6674	49.9152
FF	EFSM	9.1061	10.7218	15.5826	23.2429	31.6538	32.8922	33.4360	37.2004	43.8579
	(m,n)	(1,1)	(1,2)	(1,3)	(1,4)	(2,1)	(2,2)	(1,5)	(2,3)	(2,4)
	CFS [3]	9.1061	10.7218	15.5826	23.2429	31.6538	32.8922	33.4360	37.2004	43.8579
FS	EFSM	9.5902	13.3463	20.3423	30.1061	32.0344	35.1634	41.0123	41.9810	49.1758
	(m,n)	(1,1)	(1,2)	(1,3)	(1,4)	(2,1)	(2,2)	(2,3)	(1,5)	(2,4)
	CFS [3]	9.5902	13.3463	20.3423	30.1061	32.0344	35.1634	41.0123	41.9810	49.1758
SS	EFSM	11.3961	17.5055	26.7944	33.5896	38.3847	38.3847	45.8969	51.5392	55.5860
	(m,n)	(1,1)	(1,2)	(1,3)	(2,1)	(1,4)	(2,2)	(2,3)	(1,5)	(2,4)
	CFS [3]	11.3961	17.5055	26.7944	33.5896	38.3847	38.3847	45.8969	51.5392	55.5860

Table 2

Comparison of the dimensionless natural frequencies $\bar{\omega} = \omega_n h\sqrt{\rho / 23.2\times 10^6}$ Levy-type square orthotropic plate with boundary condition SS when $L_x / h = 10, K = 5/6$.

(m,n)	Present EFSM	CFS [1]		
	FSDT	FSDT	HSDT	3D Elasticity Theory
(1,1)	0.0474	0.0474	0.0474	0.0474
(2,1)	0.10315	0.1032	0.1033	0.1033
(1,2)	0.11870	0.1187	0.1189	0.1188
(2,2)	0.16915	0.1692	0.1695	0.1694
(3,1)	0.18835	0.1884	0.1888	0.1888
(1,3)	0.21771	0.2178	0.2184	0.2180
(3,2)	0.24688	0.2469	0.2477	0.2475
(2,3)	0.26187	0.2619	0.2629	0.2624
(4,1)	0.29583	0.2959	0.2969	0.2969

To draw mode shapes of the moderately thick plate, use is made of dynamic shape functions ($N^{\mathrm{T}}_{Wnm}, N^{\mathrm{T}}_{\Phi xnm}$ and $N^{\mathrm{T}}_{\Phi ynm}$) corresponding to spectral-modal displacement (W_{nm}, Φ_{xnm} and Φ_{ynm}), as presented in Section 3.2.3. The mode shapes for the second mode ($m = 2$) and the second root of the stiffness matrix ($n = 2$) are plotted. Figs. 5(a)-5(c) show mode shapes for the transverse displacement, rotational displacement about the x axis and rotational displacement about the y axis, respectively. It should be noted that according to Eqs. (8), variation of W_{nm} and Φ_{xnm} along the y axis is in sine form and variation of Φ_{ynm} is in cosine form.

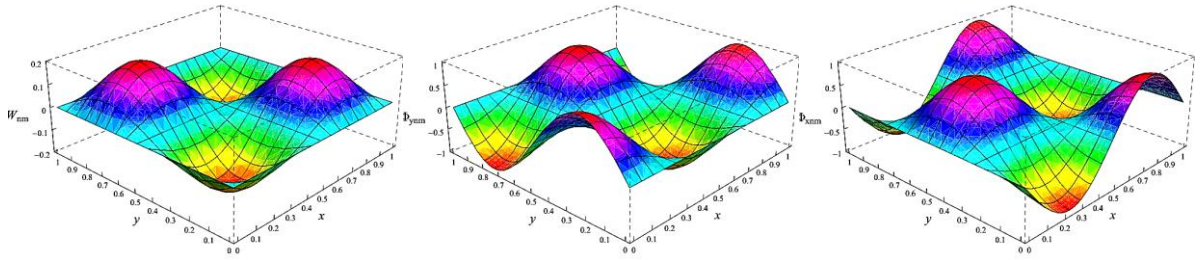

(a) W_{nmv} (b) Φ_{xnm} (c) Φ_{ynm}

Fig.5
Mode shapes (2, 2) of the Levy-type square plate with boundary conditions SS.

5.2 Forced vibration

5.2.1 Frequency response functions (FRF)

For the purpose of drawing the frequency response functions, the value of these functions must be computed for each discrete frequency. A square plate having two opposite edges simply supported and remaining edges with any arbitrary boundary conditions with geometric and mechanical properties shown in Fig. 6 is considered. Also, these plate has the mechanical properties $E_{22} = 5\times 10^9 Pa, E_{11} = 14\ E_{22}, G_{12} = 0.5\ E_{22}, G_{13} = 0.5\ E_{22}, G_{23} = 0.2\ E_{22}, \nu_{12} = 0.25$ .The plate is subjected to a concentrated dynamic load at the center of plate.

The spectral transverse displacements W_n at the center of plate for the contributions of the various numbers of half-wavelengths in y-direction are shown in Figs. 7(a)-7(b) for boundary conditions CC and SS, respectively. As shown in Fig. 7, to achieve the convergence of dynamic response in higher frequencies, it is required to consider greater numbers of half-wavelengths (m).

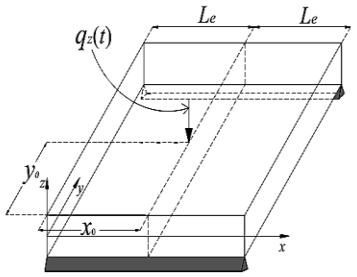

$\rho = 1500\, kg/m^3$
$K = 5/6$
$L_y = L_x = 2m$
$h = 0.1m$
$x_0 = L_e = L_x/2$

Fig.6
Levy-type square plate subjected to concentrated load at the center of plate.

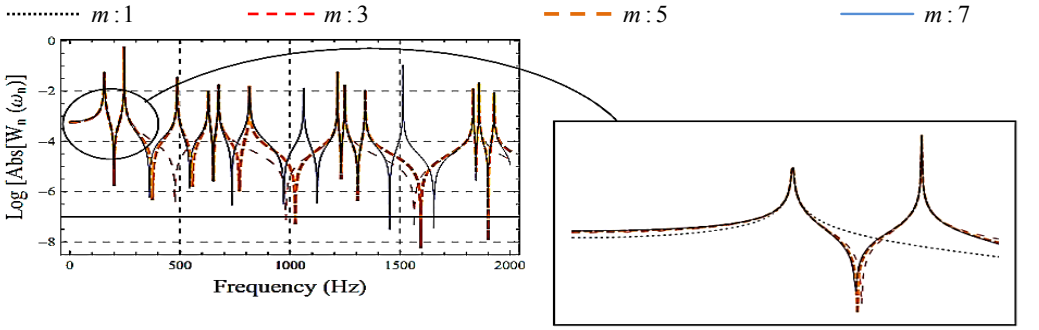

(a) CC

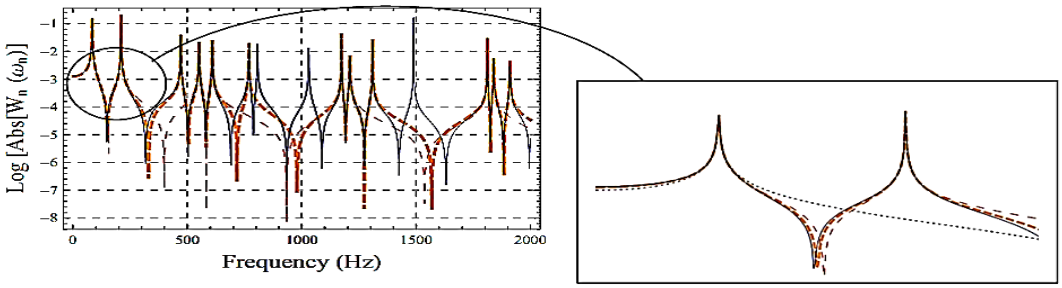

(b) SS

Fig.7
Frequency response functions (FRF) at the center of the Levy-type square orthotropic plate ($x = L_x/2, y = L_y/2$) subjected to a concentrated dynamic load.

5.2.2 Periodic loads

If the DFT coefficients are calculated for a periodic function, it can be seen that the coefficients in the frequency range $\omega_{N/2} \le \omega_n \le \omega_N$ are complex conjugates of values of this transformation in the frequency range $0 \le \omega_n \le \omega_{N/2}$. The frequency $\omega_{n=N/2}$ is known as the Nyquist frequency.

$$\omega_{n=N/2} = \omega_{Nq} = \frac{N\pi}{T} = \frac{\pi}{\Delta t}(\text{rad}/\text{s}) \quad \text{or} \quad f_{Nq} = \frac{N}{2T} = \frac{1}{2\Delta t}(\text{Hz}) \tag{51}$$

If $f_{\max}$ is the highest frequency of an actual signal, to achieve DFT coefficients with sufficient accuracy, the *Nyquist* frequency $f_{Nq} = 1/2\Delta t$ must be equal to or larger than maximum frequency [37]. This condition (in other words Nyquist condition) for sampling time interval Δt brings about some limitations, as follows:

$$\Delta t \le 1/\left(2 f_{\max}\right) \tag{52}$$

In the study of dynamic responses of plate under periodic and nonperiodic dynamic loads, the frequency domain responses W_n, Φ_{yn} and Φ_{xn} cannot be directly obtained as the complex conjugates about the Nyquist frequency. Therefore, to compute the correct time domain response w_0, ϕ_y and ϕ_x by the inverse DFT, it is just enough to calculate the DFT coefficients up to the frequency $\omega_{N/2}$ and the frequencies from $\omega_{(N/2)+1}$ up to ω_{N-1}, with respect to Eq. (53).

$$X_{N-n} = X_n^* \tag{53}$$

where X_n is the DFT coefficients. The asterisk symbol "*" is used to denote the complex conjugate of a complex number. Sometimes, it is possible to arbitrarily consider the sampling time T_s more than the period T of the periodic function. However, it should be noted that to prevent the occurrence of Leakage error, sampling time must be an integer multiple of the period [37]. Finally, according to Eq. (52), the number of samples required N_{req} in the time domain can be calculated.

$$N_{req} = T_s / \Delta t = 2 T_s f_{\max} \tag{54}$$

It should be noted that, during propagation wave the zero frequency components are undetermined; hence, by applying the null initial conditions, these components are obtained as follows [21].

$$w_0(x,y,0) = \sum_{n=0}^{N-1} W_n(x,y,\omega_n) = 0 \rightarrow W_0(x,y,\omega_0) + \sum_{n=1}^{N-1} W_n(x,y,\omega_n) = 0 \rightarrow W_0 = -\sum_{n=1}^{N-1} W_n \tag{55}$$

Consider the plate shown in Fig. 6 under a concentrated harmonic load. The variations of harmonic load over the time are sinusoidal $q_z(t) = Q_0 \sin(\omega t)$ where ω is circular frequency equal to 100π $rad/\sec$. The highest cycle frequency of load applied is $f_{\max} = \omega/2\pi = 50$ Hz; thus the required minimum number of samples with respect to Eq. (54) must be larger than $N_{req} = 100 T_s$. In this problem, the sampling time T_s is considered twice the period $T = 2\pi/\omega = 0.02$ of the periodic load. Therefore, the choice of the number of samples $N = 16 \succ N_{req} = 4$ satisfies Nyquist condition and prevents the leakage error.

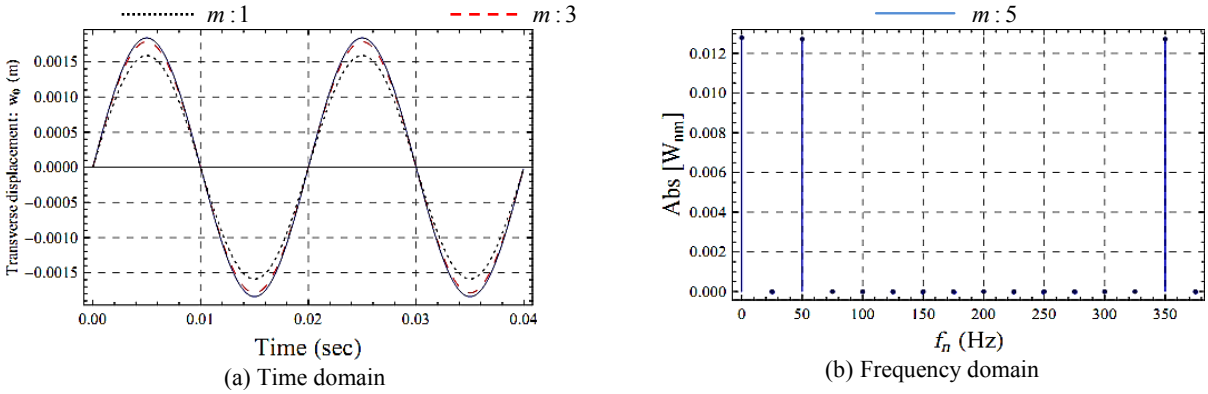

(a) Time domain (b) Frequency domain

Fig.8
Convergence of the transverse displacement of the Levy-type square orthotropic plate center subjected to a concentrated harmonic load at the center of plate for case SS.

Dynamic responses of the plate under harmonic load in the frequency domain and time domain for boundary conditions SS are presented in Fig. 8. As shown in Fig. 8(b), the DFT provides an accurate frequency spectrum from dynamic response of the plate under harmonic load with a unique spectral peak at $50Hz$. The spectral peak at

$350Hz$ is complex conjugates of the spectral peak at $50Hz$. As seen in Fig. 8(b), there is a nonzero W_{nm} at zero frequency which is due to the satisfaction of the null initial conditions [21]. The time history of the transverse displacements w_0 at the center of plate for the contributions of the various numbers of half-wavelengths in *y*-direction (*m*: 1, 3, 5) are shown in Figs. 8(a). It should be noted that in order to improve interpolation, more samples $N=1000$ are used during the sampling time. Fig. 8(a) shows that with five half-wavelengths in direction *y* axis, a reasonable representation of the dynamic responses is provided.

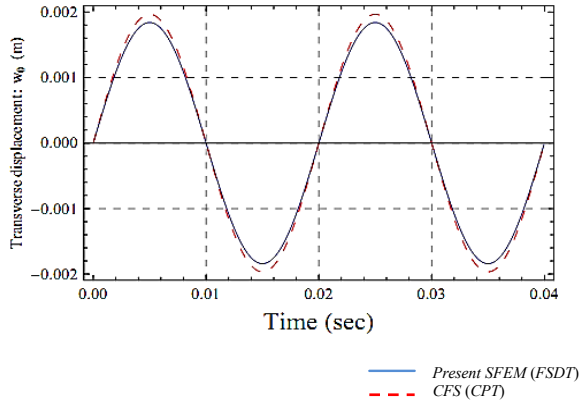

Fig.9
Comparison of the transverse displacement of the center of Levy-type square orthotropic plate subjected to a concentrated harmonic load at the center of plate for case SS.

In Fig. 9, the transverse displacements of the center of the plate calculated by the formulations developed by Szilard [38] based on CPT and present SFEM are shown. Szilard use a CFS for the dynamic analysis. The transverse displacements shown in the figure have been obtained with the contributions of five half-wavelengths in *y*-direction. The effect of shear deformation on the transverse displacement obtained by SFEM based on FSDT and CPT is shown in Fig. 9. Among the advantages of the SFEM compared with CFS, one can mention the development capability of this approach for all boundary conditions, the assembly plates, the plate structures and more complicated loading conditions.

5.2.3 Impulsive loads

Since in the vibration of plates usually we are faced with nonperiodic dynamic loads (i.e. impulsive load), consider the plate shown in Fig. 6 under a concentrated impulsive load of rectangular-shape. The duration of impulsive load, as shown in Fig. 10(a), is equal $t_d = 0.1\text{sec}$. To obtain the spectral nodal forces vector, we must transform the load applied from the time domain into the frequency domain by DFT, as shown in Fig, 10(b). It should be noted that the DFT is symmetric about the middle or Nyquist frequency, but to make the frequency domain responses clearer, only a part of the frequency domain is considered. As we know, the highest frequency of the impulsive loads is infinite. The sampling time interval required to satisfy the Nyquist conditions is $\Delta t = 0$ sec, which is not possible in practice. To obtain the appropriate sampling time interval, we should select several highest frequencies to investigate the convergence of the dynamic responses. In this example, three values of 100, 250, 500 and 1000 *Hz* for the maximum frequency are selected. Given Eq. (52), the sampling time interval obtained is equal to 0.005, 0.002, 0.001 and 0.0005 seconds.

The convergence of the dynamic responses of the plate under impulsive load of rectangular-shape in the time domain for boundary conditions SS is presented in Fig. 11. In this figure, the transverse displacements w_0 at the center of the plate for various values of the sampling time interval ($\Delta t = 0.005, 0.002, 0.001, 0.0005$) are shown. Fig. 11 shows that with the sampling time interval $\Delta t = 0.001$ a reasonable representation of the dynamic responses could be provided.

In Fig. 12, the results in frequency domain for sampling time interval $\Delta t = 0.0005$ are presented. Along with the frequency domain dynamic responses, the variation of dynamic stiffness matrix determinant in logarithmic scale with respect to discrete frequencies is plotted. As expressed in Section 5.3, points which tend the logarithmic function toward negative infinity represent the natural frequencies of the plate. The frequency peak of frequency domain dynamic responses in Fig. 12 represents the resonance of responses in the natural frequency of the plate.

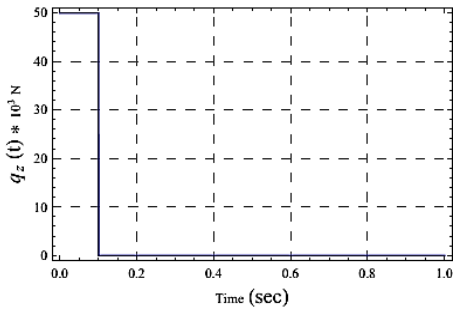

(a) Time domain

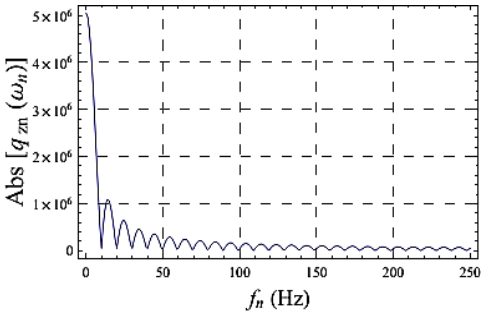

(b) Frequency domain

Fig.10
Impulsive load of rectangular shape in the time and frequency domain.

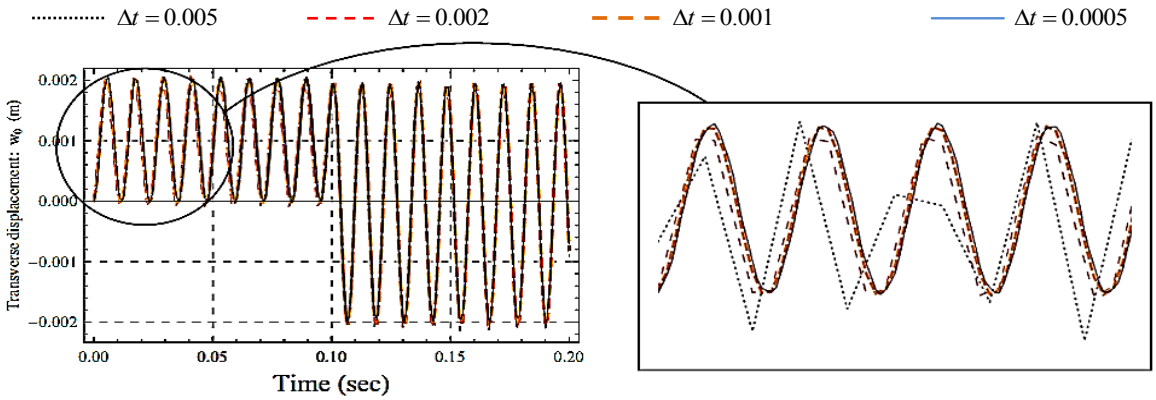

Fig.11
Convergence of the transverse displacement of the Levy-type square orthotropic plate center subjected to a concentrated impulsive load of rectangular-shape at the center of plate for case SS.

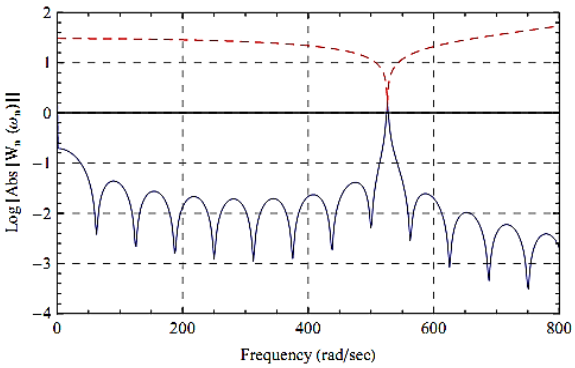

Fig.12
Transverse displacement of the Levy-type square orthotropic plate center subjected to a concentrated impulsive load of rectangular-shape at the center of plate for case SS in frequency domain.

The only solution available to the dynamic responses in the time domain is by using CFS just for simply supported boundary conditions on all edges of the plate (Navier's solution). The time history of the transverse displacement w_0 at the center of the plate obtained by SFEM based on FSDT and analytical solution (CFS) based on CPT is shown in Fig. 13. Comparative results of Reddy [35] are obtained from the solution of the formulation presented in this references and programming the algorithm desired in the environment of Mathematica software. One of the advantages of the SFEM, compared with CFS, is the capability of this approach for modelling complicated loading conditions. This method also has the analytical ability of the stepped thickness plates, plates with internal support and plates with discontinuous or irregular mechanical properties.

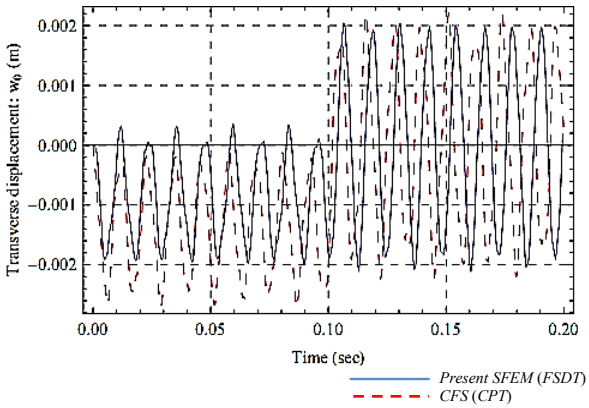

Fig.13
Comparison of transverse displacement of the Levy-type square orthotropic plate center subjected to a concentrated impulsive load of rectangular-shape at the center of plate for case SS.

Since in the SFEM, the dynamic shape functions are obtained from the exact solution of the governing differential equations, it is possible to exactly obtain the displacement variables at any moment of vibration for any arbitrary point of plate. For example, the transverse displacement of the total surface of the plate is plotted at the moment when maximum transverse displacement at point $x = L_x/4, y = L_y/4$ of plate occurs in Fig. 14 for the plate described above for different boundary conditions. Note that the location of load applied from the center of the plate to the point $x = L_x/4, y = L_y/4$ of the plate was changed. In Fig. 14, the horizontal axes are given per meters and vertical axis per *mm*.

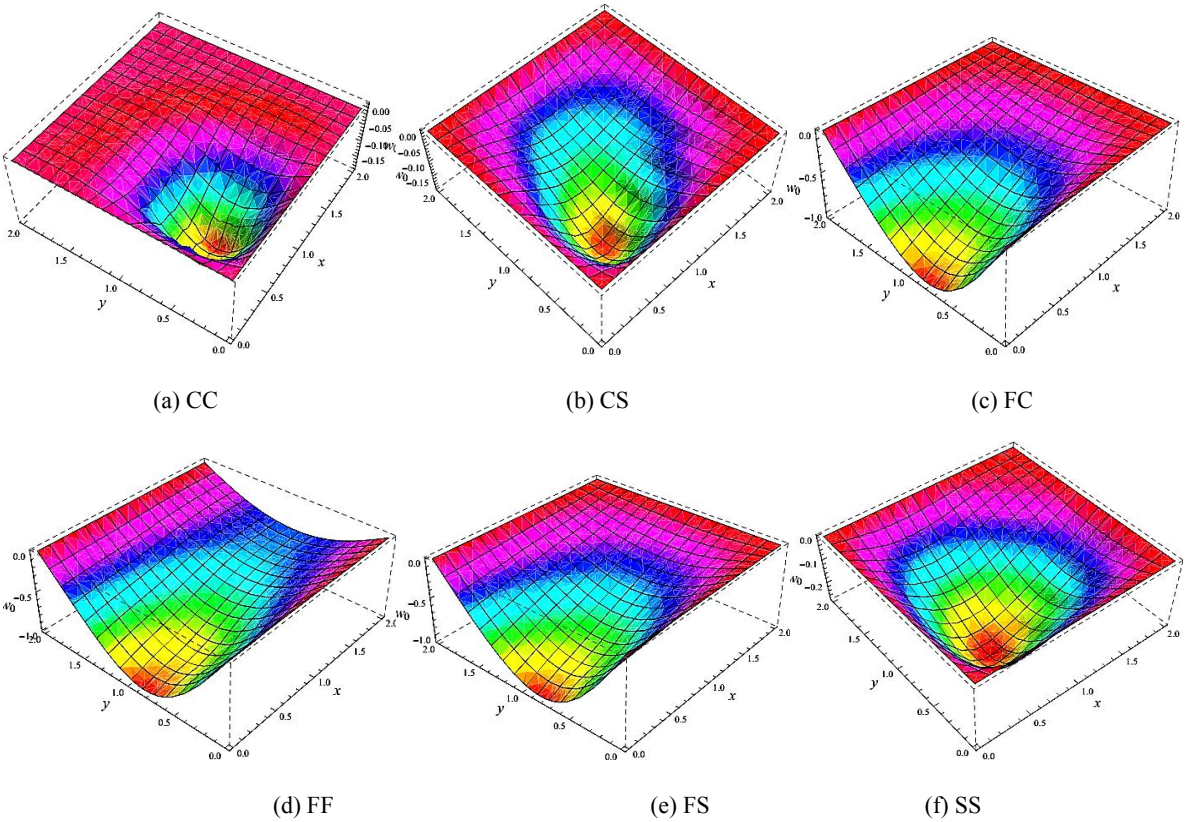

Fig.14
Maximum transverse displacement of the Levy-type moderately thick square plate subjected to a concentrated impulsive load of rectangular shape at point $x = L_x/4, y = L_y/4$ of plate for all boundary conditions.

6 CONCLUSIONS

The transverse vibration of the moderately thick orthotropic rectangular plates of Levy-type by the SFEM based on FSDT was modeled. Since the frequency-dependent dynamic shape functions in SFEM is obtained from the exact solution of the governing differential equations of motion of the plate, increasing the number of spectral element to achieve the exact answers is not required. In this study, the results obtained by the spectral finite element formulation use maximum of two finite elements in *x*-direction. As is noticeable, the proposed SFEM achieves exact results with minimal finite elements, compared with CFS. Therefore, it is possible to effectively use this procedure for the plate structures and other plates in which more than one finite element is needed for modeling purposes.

DFT is used to obtain frequency domain and time domain dynamic responses. The dynamic responses to impulsive loads were obtained. The extremely high accuracy of the present SFEM was verified by comparing it with CFS. The results obtained in the present paper can serve as a benchmark for verifying other analytical and numerical methods.

REFERENCES

[1] Reddy J.N., Phan N.D., 1985, Stability and vibration of isotropic, orthotropic and laminated plates according to a higher-order shear deformation theory, *Journal of Sound and Vibration* **98**(2): 157-170.

[2] Xiang Y., Wei G.W., 2004, Exact solutions for buckling and vibration of stepped rectangular Mindlin plates, *International Journal of Solids and Structures* **41**: 279-294.

[3] Hosseini-Hashemi Sh., Arsanjani M., 2005, Exact characteristic equations for some of classical boundary conditions of vibrating moderately thick rectangular plates, *International Journal of Solids and Structures* **42**: 819-853.

[4] Hosseini-Hashemi Sh., Fadaee M., Eshaghi M., 2010, A novel approach for in-plane/out-of-plane frequency analysis of functionally graded circular/annular plates, *International Journal of Mechanical Sciences* **52**: 1025-1035.

[5] Hosseini-Hashemi Sh., Rokni Damavandi Taher H., Akhavan H., Omidi M., 2010, Free vibration of functionally graded rectangular plates using first-order shear deformation plate theory, *Applied Mathematical Modelling* **34**: 1276-1291.

[6] Hosseini-Hashemi Sh., Fadaee M., Atashipour, S.A., 2011, A new exact analytical approach for free vibration of Reissner–Mindlin functionally graded rectangular plates, *International Journal of Mechanical Sciences* **53**: 11-22.

[7] Hosseini-Hashemi Sh., Fadaee M., Atashipour S.A., 2011, Study on the free vibration of thick functionally graded rectangular plates according to a new exact closed-form procedure, *Composite Structure* **93**: 722-735.

[8] Hosseini-Hashemi Sh., Fadaee M., Rokni Damavandi Taher H., 2011, Exact solutions for free flexural vibration of Lévy-type rectangular thick plates via third-order shear deformation plate theory, *Applied Mathematical Modelling* **35**: 708-727.

[9] Akhavan H., Hosseini-Hashemi Sh., Rokni Damavandi Taher H., Alibeigloo A., Vahabi Sh., 2009, Exact solutions for rectangular Mindlin plates under in-plane loads resting on Pasternak elastic foundation. Part II: frequency analysis, *Computational Materials Science* **44**: 951-961.

[10] Hatami S., Azhari M., Saadatpour M.M., 2007, Free vibration of moving laminated composite plates, *Composite Structures* **80**: 609-620.

[11] Hatami S., Ronagh H.R., Azhari M., 2008, Exact free vibration analysis of axially moving viscoelastic plates, *Computers and Structures* **86**: 1738-1746.

[12] Boscolo M., Banerjee J.R., 2011, Dynamic stiffness elements and their applications for plates using first order shear deformation theory, *Computers and Structures* **89**: 395-410.

[13] Boscolo M., Banerjee J.R., 2012, Dynamic stiffness formulation for composite Mindlin plates for exact modal analysis of structures. Part I: Theory, *Computers and Structures* **96-97**: 61-73.

[14] Boscolo M., Banerjee J.R., 2012, Dynamic stiffness formulation for composite Mindlin plates for exact modal analysis of structures. Part II: Results and application, *Computers and Structures* **96-97**: 74-83.

[15] Leung A.Y.T., Zhou W.E., 1996, Dynamic stiffness analysis of laminated composite plates, *Thin-Walled Structures* **25**(2): 109-133.

[16] Fazzolari F.A., Boscolo M., Banerjee J.R., 2013, An exact dynamic stiffness element using a higher order shear deformation theory for free vibration analysis of composite plate assemblies, *Composite Structures* **96**: 262-278.

[17] Kolarevic N., Nefovska-Danilovic M., Petronijevic M., 2015, Dynamic stiffness elements for free vibration analysis of rectangular Mindlin plate assemblies, *Journal of Sound and Vibration* **359**: 84-106.

[18] Kolarevic N., Marjanovic M., Nefovska-Danilovic M., Petronijevic M., 2016, Free vibration analysis of plate assemblies using the dynamic stiffness method based on the higher order shear deformation theory, *Journal of Sound and Vibration* **364**: 110-132.

[19] Ghorbel O., Casimir J.B., Hammami L., Tawfiq I., Haddar M., 2015, Dynamic stiffness formulation for free orthotropic plates, *Journal of Sound and Vibration* **346**: 361-375.

[20] Ghorbel O., Casimir J.B., Hammami L., Tawfiq I., Haddar M., 2016, In-plane dynamic stiffness matrix for a free orthotropic plate, *Journal of Sound and Vibration* **364**: 234-246.
[21] Doyle J.F., 1997, *Wave Propagation in Structures: Spectral Analysis Using Fast Discrete Fourier Transforms*, Springer-Verlag, New York, Second Edition.
[22] Lee U., Lee J., 1998, Vibration analysis of the plates subject to distributed dynamic loads by using spectral element method, *KSME International Journal* **12**(4): 565-571.
[23] Kim J., Cho J., Lee U., Park, S., 2003, Modal spectral element formulation for axially moving plates subjected to in-plane axial tension, *Computers and Structures* **81**: 2011-2020.
[24] Chakraborty A., Gopalakrishnan S., 2005, A spectrally formulated plate element for wave propagation analysis in anisotropic material, *Computer Methods in Applied Mechanics and Engineering* **194**: 4425-4446.
[25] Kwon K., Lee U., 2006, Spectral element modeling and analysis of an axially moving thermo elastic beam-plate, *Journal of Mechanics of Materials and Structures* **1**: 605-632.
[26] Wang G., Unal A., 2013, Free vibration of stepped thickness rectangular plates using spectral finite element method, *Journal of Sound and Vibration* **332**: 4324-4338.
[27] Hajheidari H., Mirdamadi H.R., 2012, Free and transient vibration analysis of an un-symmetric cross-ply laminated plate by spectral finite elements, *Acta Mechanica* **223**: 2477-2492.
[28] Hajheidari H., Mirdamadi H.R., 2013, Frequency-dependent vibration analysis of symmetric cross-ply laminated plate of Levy-type by spectral element and finite strip procedures, *Applied Mathematical Modelling* **37**: 7193-7205.
[29] Liu X., Banerjee J.R., 2015, An exact spectral-dynamic stiffness method for free flexural vibration analysis of orthotropic composite plate assemblies. Part I: Theory, *Composite Structures* **132**: 1274-1287.
[30] Liu X., Banerjee J.R., 2015,An exact spectral-dynamic stiffness method for free flexural vibration analysis of orthotropic composite plate assemblies . Part II: Applications, *Composite Structures* **132**: 1288-1302.
[31] Liu X., Banerjee J.R., 2016, Free vibration analysis for plates with arbitrary boundary conditions using a novel spectral-dynamic stiffness method, *Computers & Structures* **164**: 108-126.
[32] Park I., Lee U., 2015, Spectral element modeling and analysis of the transverse vibration of a laminated composite plate, *Composite Structures* **134**: 905-917.
[33] Shirmohammadi F., Bahrami S., Saadatpour M.M., Esmaeily A., 2015, Modeling wave propagation in moderately thick rectangular plates using the spectral element method, *Applied Mathematical Modelling* **39**(12): 3481-3495.
[34] Bahrami S., Shirmohammadi F., Saadatpour M.M., 2015, Modeling wave propagation in annular sector plates using spectral strip method, *Applied Mathematical Modelling* **39**(21): 6517-6528.
[35] Reddy J.N., 2007, *Theory and Analysis of Elastic Plates and Shells*, CRC Press, Boca Raton, Second Edition.
[36] Reissner, E., 1944, On the theory of bending of elastic plates, *Journal Math Physics* **23**(4): 184-191.
[37] Lee U., 2009, *Spectral Element Method in Structural Dynamics*, John Wiley & Sons.
[38] Szilard R., 2004, *Theories and Applications of Plate Analysis: Classical, Numerical and Engineering Methods*, John wiley & Sons, Inc, New Jersey.